Kathryn M. Olesnavage
Global Engineering and Research (GEAR) Laboratory,
Department of Mechanical Engineering,
Massachusetts Institute of Technology,
Cambridge, MA 02139
e-mail: kolesnav@mit.edu

Victor Prost
Global Engineering and Research (GEAR) Laboratory,
Department of Mechanical Engineering,
Massachusetts Institute of Technology,
Cambridge, MA 02139
e-mail: vprost@mit.edu

William Brett Johnson
Global Engineering and Research (GEAR) Laboratory,
Department of Mechanical Engineering,
Massachusetts Institute of Technology,
Cambridge, MA 02139
e-mail: wbj@mit.edu

Amos G. Winter, V[1]
Global Engineering and Research (GEAR) Laboratory,
Department of Mechanical Engineering,
Massachusetts Institute of Technology,
Cambridge, MA 02139
e-mail: awinter@mit.edu

Passive Prosthetic Foot Shape and Size Optimization Using Lower Leg Trajectory Error

A method is presented to optimize the shape and size of a passive, energy-storing prosthetic foot using the lower leg trajectory error (LLTE) as the design objective. The LLTE is defined as the root-mean-square error between the lower leg trajectory calculated for a given prosthetic foot's deformed shape under typical ground reaction forces (GRFs), and a target physiological lower leg trajectory obtained from published gait data for able-bodied walking. Using the LLTE as a design objective creates a quantitative connection between the mechanical design of a prosthetic foot (stiffness and geometry) and its anticipated biomechanical performance. The authors' prior work has shown that feet with optimized, low LLTE values can accurately replicate physiological kinematics and kinetics. The size and shape of a single-part compliant prosthetic foot made out of nylon 6/6 were optimized for minimum LLTE using a wide Bezier curve to describe its geometry, with constraints to produce only shapes that could fit within a physiological foot's geometric envelope. Given its single part architecture, the foot could be cost effectively manufactured with injection molding, extrusion, or three-dimensional printing. Load testing of the foot showed that its maximum deflection was within 0.3 cm (9%) of finite element analysis (FEA) predictions, ensuring the constitutive behavior was accurately characterized. Prototypes were tested on six below-knee amputees in India—the target users for this technology—to obtain qualitative feedback, which was overall positive and confirmed the foot is ready for extended field trials. [DOI: 10.1115/1.4040779]

1 Introduction

The aim of this work was to develop a framework to optimize the design of a single-part compliant prosthetic foot to best replicate physiological lower leg trajectory when typical loads are applied, then use this framework to design and build a low-cost, mass-manufacturable prosthetic foot. This study was motivated by Bhagwan Mahaveer Viklang Sahayata Samiti (BMVSS), an organization based in Jaipur, India, that distributes approximately 26,000 units of its prosthetic foot, the Jaipur Foot, each year[2]. The Jaipur Foot was designed to meet the needs of persons with amputations living in India. It can withstand harsh environmental conditions (such as barefoot use and submersion in water); it looks like a biological foot to help users avoid social stigmas against mobility aids, and it permits culturally specific activities (such as squatting). The Jaipur Foot costs approximately $10 USD to make, but is given to users for free through donations and government subsidies that fund BMVSS. It is generally regarded as a high-performing prosthetic foot, not only in the context of emerging markets but also compared to feet many times more expensive [1]. However, the Jaipur Foot is handmade, which leads to quality variation. It is also much heavier (at approximately 1000 g for a 27 cm foot) than other low-cost passive prosthetic feet, such as the SACH foot (at 625 g)[3]. The goal of this work is ultimately to design a prosthetic foot that facilitates near-able-bodied walking kinematics to avoid stigmas associated with disability, is lighter than the Jaipur Foot, costs no more than $10 USD to produce, and can be mass-manufactured to maintain product uniformity. The present study focuses on the foundation of this endeavor: the creation of a low-cost, single-part, energy-storing, plastic keel that can fit within a cosmetic covering.

Connecting the geometry and stiffness of the keel to the anticipated kinematics and kinetics of the user is critical for designing a prosthetic foot with a desired biomechanical performance. Numerous studies have shown that the mechanical design of a passive prosthetic foot affects the users' gait [2–9]. However, there is no consensus on exactly how the mechanical properties of a foot relate to its biomechanical performance [10–13]. Without this relationship, it is impossible to optimize the design of a prosthetic foot for peak performance, or to evaluate potential tradeoffs when designing low-cost feet for emerging markets with minimal sacrifice of performance.

One proposed design objective for prosthetic feet is to replicate physiological roll-over geometries. The roll-over geometry of a foot is defined as the path of the center of pressure along the bottom of the foot from heel strike to opposite heel strike as measured in the ankle-knee reference frame [14]. It has been shown that roll-over geometries are fairly consistent for individuals with similar leg lengths, and that roll-over geometries remain unchanged through variations in walking speed, shoe heel height, and carried torso weight [15–17]. Because the roll-over geometry can be measured both mechanically for a prosthetic foot without a human subject that inherently introduces variability, and for typical, unimpaired walking for biological feet, it provides a connection between the mechanical properties of the foot and gait mechanics that can be utilized to optimize prosthetic feet to better replicate physiological functionality. However, the roll-over geometry is measured only in the ankle-knee reference frame and does not include any information about the orientation of this

[1]Corresponding author.
[2]JaipurFoot.org
[3]https://professionals.ottobockus.com/

Contributed by the Mechanisms and Robotics Committee of ASME for publication in the Journal of Mechanical Design. Manuscript received November 6, 2017; final manuscript received June 11, 2018; published online July 31, 2018. Assoc. Editor: Massimo Callegari.

reference frame relative to the global reference frame. Nor does it include temporal effects of a leg's progression through a step. Thus, roll-over geometry does not fully describe the functionality of a given prosthetic foot. Our previous work has demonstrated that it is possible for two different prosthetic feet to have identical roll-over geometries but yield very different lower leg kinematics under the same ground reaction forces (GRFs) [18–20]. Therefore, roll-over geometry is insufficient to be used in optimizing the design of prosthetic feet, as ideal kinematics cannot be ensured.

We have created a novel design objective, called the lower leg trajectory error (LLTE), that quantifies how closely the position of the lower leg segment for a given prosthetic foot is able to replicate target physiological lower leg position, in both space and time, throughout the course of a step [18–20]. LLTE is defined as

$$\mathrm{LLTE} \equiv \left[\frac{1}{N}\sum_{n=1}^{N}\left\{\left(\frac{x_{\mathrm{knee},n}^{\mathrm{model}}-x_{\mathrm{knee},n}^{\mathrm{phys}}}{\bar{x}_{\mathrm{knee}}^{\mathrm{phys}}}\right)^2+\left(\frac{y_{\mathrm{knee},n}^{\mathrm{model}}-y_{\mathrm{knee},n}^{\mathrm{phys}}}{\bar{y}_{\mathrm{knee}}^{\mathrm{phys}}}\right)^2+\left(\frac{\theta_{LL,n}^{\mathrm{model}}-\theta_{LL,n}^{\mathrm{phys}}}{\bar{\theta}_{LL}^{\mathrm{phys}}}\right)^2\right\}\right]^{\frac{1}{2}} \tag{1}$$

where $x_{\mathrm{knee},n}^{\mathrm{model}}$ and $y_{\mathrm{knee},n}^{\mathrm{model}}$ are the horizontal and vertical positions of the knee and $\theta_{\mathrm{knee},n}^{\mathrm{model}}$ is the orientation of the lower leg segment with respect to vertical, as calculated for a modeled prosthesis under an assumed set of ground reaction force and center of pressure data at the nth time interval, where stance phase is divided into a total of N intervals. The variables $x_{\mathrm{knee},n}^{\mathrm{phys}}$, $y_{\mathrm{knee},n}^{\mathrm{phys}}$, and $\theta_{LL,n}^{\mathrm{phys}}$ refer to the same values as measured for target able-bodied walking, and $\bar{x}_{\mathrm{knee}}^{\mathrm{phys}}$, $\bar{y}_{\mathrm{knee}}^{\mathrm{phys}}$, and $\bar{\theta}_{LL}^{\mathrm{phys}}$ are the mean physiological values over all N time intervals, which serve to normalize the errors in each variable. Each of these variables refers to the global, or lab-based, reference frame, as shown in Fig. 1. Throughout this work, all physiological gait data came from Winter's published data, which were obtained from a subject of body mass 56.7 kg and leg length 0.83 m [21].

The focus of this work is not the definition of LLTE as a cost function for designing prosthetic feet, but rather developing a framework that can be used to design a prosthetic foot to meet specific needs while minimizing the value of a cost function. A detailed discussion of why this particular cost function, including the selection of the specific variables and normalization factors in Eq. (1), produces a foot that best replicates physiological gait kinematic and kinetic data can be found in Refs. [18] and [20]. However, the framework could similarly be employed with a different cost function to optimize the foot for other goals.

Three simple prosthetic foot architectures, each with two degrees-of-freedom (2 DoF), have previously been optimized using LLTE to demonstrate its usefulness as a design tool. The first model was a rigid circular foot, with the radius of the circle, R, and the horizontal position of the center of the circle, x_c, as design variables (Fig. 2(*a*)). The second consisted of rotational pin joints at the ankle and metatarsal joints, with the rotational stiffness of each joint, k_{ank} and k_{met}, as the design variables (Fig. 2(*b*)). The third and final model considered also consisted of a rotational ankle joint, but replaced the metatarsal joint with a compliant cantilever beam forefoot, with the ankle stiffness, k_{ank}, and the forefoot beam bending stiffness, EI (where E is the modulus of elasticity and I is the area moment of inertia), as design variables (Fig. 2(*c*)). Multiple prototypes based on these simple architectures have been built and used in clinical testing to validate the LLTE optimization method [20,22,23]. We have shown in prior work that prosthetic foot prototypes with LLTE values near optimum are able to promote gait symmetry and accurately replicate both physiological kinematics and kinetics, and that feet with larger LLTE values induce compensatory behaviors that

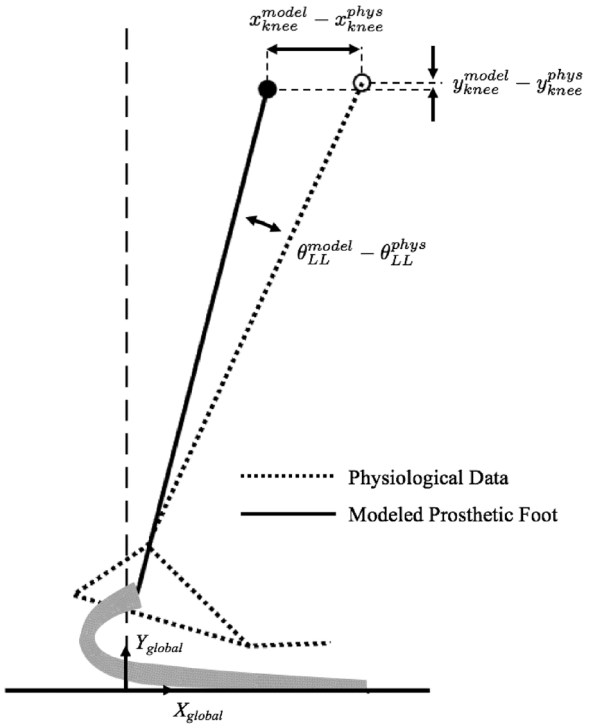

Fig. 1 Lower leg position for modeled prosthetic foot (solid line) and target physiological gait data (dotted line) at one particular time interval during a step, with variables used in Eq. (1) shown. Note that physiological data come from markers placed at anatomically relevant positions on a human subject, resulting in a gap between the marker positions and the ground.

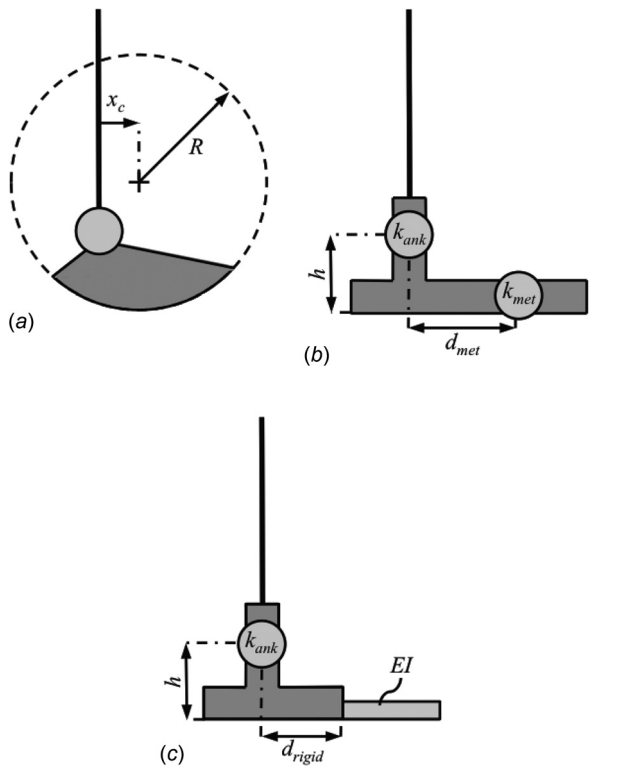

Fig. 2 Three analytical prosthetic foot architectures optimized and compared using LLTE: (*a*) rigid model, (*b*) rotational ankle and metatarsal model, and (*c*) rotational ankle, beam forefoot model

cause gait asymmetries [20,]. While the simple, two degree-of-freedom architectures have been useful tools to rapidly iterate through experimental prototypes and effectively prove the concept of prosthetic foot optimization based on LLTE, the resulting prototypes are too large to fit within a shoe, heavy (between 980 g and 2 kg), and consist of relatively complex mechanisms, with part counts on the order of 10 and moving components that would require frequent maintenance (Fig. 3). In order to translate these experimental prototypes to commercial products, a lighter, more robust, and easier to manufacture design is required.

In this work, compliant mechanism optimization techniques were used to design a single-part foot that minimizes the LLTE to best replicate physiological lower leg kinematics. The design space parametrization, based on a wide Bézier curve, is discussed, together with constraints that were applied to ensure only physically meaningful shapes were considered. The evaluation of the LLTE value for a given design using MATLAB (The MathWorks, Inc., Natick, MA) and ADINA (ADINA R & D, Inc., Watertown, MA) finite element analysis software is described. The optimal design is presented and compared to the simple analytical models previously optimized. A prosthetic foot (which will form the keel in our eventual commercial product foot with a cosmetic covering) was built based on the optimal design and tested on an Instron material testing machine (Illinois Tool Works, Inc., Norwood, MA) to show that the finite element results used in the optimization accurately represented the foot. The foot was then tested with six subjects with unilateral transtibial amputations at BMVSS' facility in Jaipur, India. Feedback indicated that, once a cosmetic and protective cover is designed for the foot, the prototype is ready for extended field trials without significant changes to the structure of the keel.

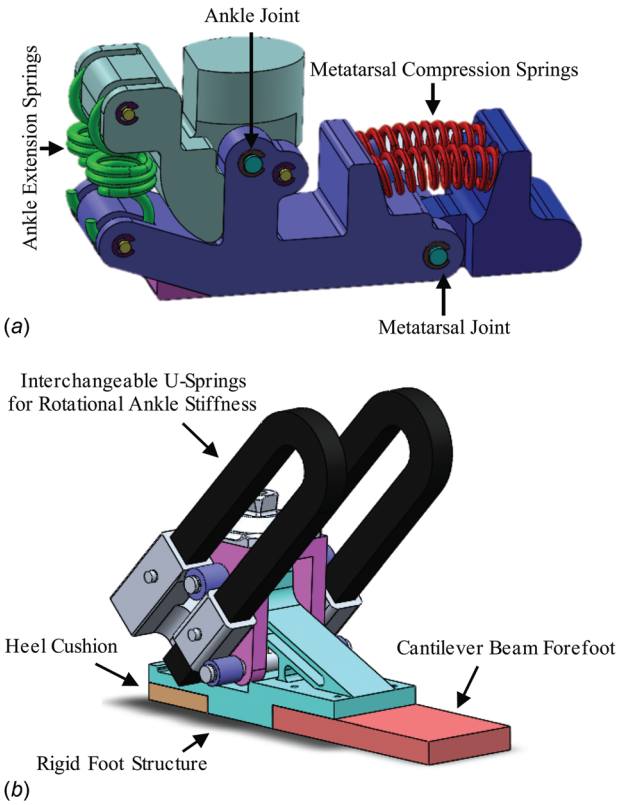

Fig. 3 Prototypes designed based on the simple prosthetic foot models shown in Fig. 2. While useful tools for clinical testing, the prototypes are too heavy, large, and complicated to be used as daily prostheses: (*a*) prototype with rotational ankle and metatarsal joints and (*b*) prototype with rotational ankle, beam forefoot.

2 Method

2.1 Size and Shape Parameterization. The goal of this work was to develop a framework to design and optimize a prosthetic foot structure consisting of a single part that, when acted upon by typical ground reaction forces, deforms in such a way as to best replicate typical lower leg kinematics, as quantified by minimizing the lower leg trajectory error. By responding to a specific loading scenario and deforming elastically to achieve a desired output motion, the foot meets the definition of a compliant mechanism [24]. Because the primary goal of this work was to develop a framework to produce an optimal prosthetic foot with minimal LLTE value, the design of the foot was kept as simple as possible for rapid implementation and iteration through the methodology. Therefore, only the design of the forefoot was optimized, as many prosthetic feet de-couple early stance from the rest of stance phase by using a separate mechanism, such as a cushion or a secondary compliant mechanism, for the heel portion of the foot. Several ways in which complexity could be added back into the design, including adding a heel in the optimization process, are discussed in Sec. 4.

There is a plethora of literature on topology synthesis and optimization for compliant mechanisms [25–31], including continuum element density approaches, frame element-based structures, and pseudo-rigid body models. However, the outputs of these topology optimizations have several practical limitations; for example, some consist only of uniform elements or uniform cross section, have unclear boundaries or checkerboard patterns, or result in localized flexural hinges with high stress concentrations [32]. Furthermore, the topology of a prosthetic foot does not need to be complicated. All that is required is material at the ankle that can be attached to the rest of the prosthesis, and a flat bottom surface of the foot upon which the center of pressure can progress smoothly from heel-strike to toe-off. What remains to be optimized is only the size and shape of the mechanism connecting the ankle to the bottom of the foot.

Several methods for compliant mechanism size and shape optimization were considered [33–35], but ultimately our foot was realized using a wide Bézier curve, as presented by Zhou and Ting [36]. A wide Bézier curve is a parametric curve with a shape dictated by a series of control points. With a Bézier curve, a cubic curve can be defined by the position of four control points, reducing a potentially complex shape to a limited number of design variables. The width of the curve is added as a variable by using control circles rather than control points and defining the width of the wide Bézier curve as a function of the diameters of these control circles. Unlike typical outputs of most topology synthesis and optimization methods, the output of the optimization method employed here is a two-dimensional extruded shape that is easily manufacturable with minimal postprocessing, which means the theoretical optimization result can be built as a physical prototype quickly and easily.

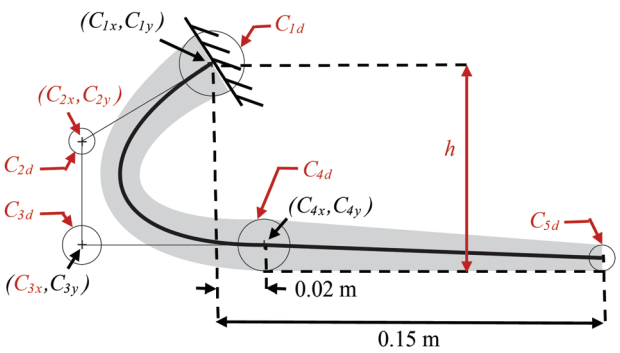

Fig. 4 Parameterization of the keel of the foot. The shape and size of the keel are defined with nine independent design variables shown in red.

The shape and width of the Bézier curve (and resulting forefoot) were defined by four control points (C_1, C_2, C_3, and C_4 in Fig. 4), each of which had an x-position, y-position, and a diameter, denoted by subscripts x, y, and d, respectively. The first node, C_1, was the point of attachment between the foot and the rest of the prosthesis, and was fixed at $(C_{1x}, C_{1y}) = (0, 0)$. Throughout the course of this work, all measurements and coordinates are in units of meters, unless otherwise stated. The height of the foot from the attachment point to the bottom of the foot was h such that $C_{4y} \equiv -h + 1/2C_{4d}$, where C_{4d} was the width of the foot at C_4. To prevent any kinks in the structure, the tangent to the Bézier curve at point C_4 was made horizontal by enforcing $C_{3y} \equiv C_{4y}$. The coordinate C_{4x} was defined by the horizontal position of the center of pressure at the first instant in Winter's published gait data for which the center of pressure was anterior to the ankle in the ankle-knee reference frame, that is, $C_{4x} = 0.02$ m. The foot extended forward from C_4 to the tip of the foot, C_5, with $C_{5x} = 0.15$ m. Together, C_{4x} and C_{5x} determined the length of the forefoot and were selected to cover the distance the center of pressure progresses in Winter's gait data from foot flat to toe-off. The width of the forefoot decreased linearly from C_4 to the tip of the foot, with the design variable ff_{frac} defining the ratio of the width of the tip of the forefoot to the width of the foot at C_4. That is, $ff_{\text{frac}} \equiv C_{5d}/C_{4d}$. In order to keep the foot flat and stable on the ground when it was unloaded, $C_{5y} \equiv -h + 1/2ff_{\text{frac}} \cdot C_{4d}$. Thus, there were nine independent design variables to be optimized

$$X = [h, C_{1d}, C_{2x}, C_{2y}, C_{2d}, C_{3x}, C_{3d}, C_{4d}, ff_{\text{frac}}] \tag{2}$$

Upper and lower bounds were imposed on each of the variables to constrain the shape and size of the structure to approximately fit within the envelope of a biological foot. The initial bounds were

$$lb = [0.06, 0.005, -0.15, -0.10, 0.005, -0.15, 0.005, 0.005, 0.1] \tag{3}$$

and

$$ub = [0.15, 0.04, 0.07, 0.10, 0.04, 0.01, 0.04, 0.04, 1] \tag{4}$$

These preliminary bounds were very loose on the variables h, C_{2x}, C_{2y}, and C_{3x} to avoid constraining the design space more than necessary. After an optimal design was found, these bounds were modified to enforce the requirement that the optimal design could not be larger than a biological foot. The thickness of the foot into the plane of the page was fixed at 0.06 m such that the foot can easily fit into a shoe or cosmesis. Examples of possible foot shapes explored through this particular parametrization are shown in Fig. 5.

2.2 Materials. The optimization was performed using nylon 6/6, with elastic modulus $E = 2.41$ GPa and yield strength $\sigma_y = 82.7$ MPa. Nylon was selected as a reasonable material choice for a low-cost prosthetic foot because the high ratio of yield strength to elastic modulus allows it to achieve a high strain energy density, and thus high deformations before yielding.

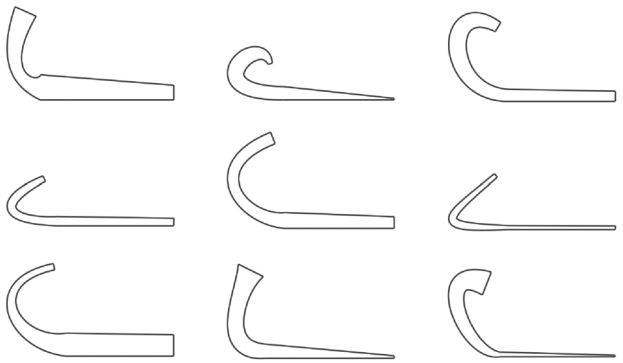

Fig. 5 Various possible keel designs that fall within the defined design space

2.3 Constraints. Particular sets of design variables could yield wide Bézier curves that intersect themselves, resulting in a shape with no physical meaning. Self-intersection occurs either when the radius of curvature of the center Bézier curve is less than half the width of the outer shape (Fig. 6(*a*)), or the center curve creates a loop (Fig. 6(*b*)). These self-intersections can be prevented with the following constraints:

$$\max(0.5w_c - \rho) \leq 0 \tag{5}$$

and

$$\left(\frac{l\overline{C_1C_2}}{l\overline{QC_1}} - \frac{4}{3}\right)\left(\frac{l\overline{C_2C_3}}{l\overline{QC_2}} - \frac{4}{3}\right) - \frac{4}{9} \leq 0 \tag{6}$$

where ρ is the radius of curvature of the center Bézier curve, Q the point of intersection of line segments $\overline{C_1C_2}$ and $\overline{C_3C_4}$, as shown in Fig. 6(*b*), and $l\overline{C_1C_2}$ is the length of the line segment between control points C_1 and C_2, and so on.

Since the size and shape parameterization defined $C_{3y} \equiv C_{4y}$ and the shape has been defined such that the bottom of the control circle C_4 is the bottom of the foot, if C_3d were greater than C_{4d}, then the foot could protrude below the intended bottom surface. Therefore, the linear inequality constraint

$$C_{3d} - C_{4d} \leq 0 \tag{7}$$

was included.

Finally, a constraint was imposed to limit the maximum stress in the foot structure

$$\sigma_{\max} - \sigma_{\text{allow}} \leq 0 \tag{8}$$

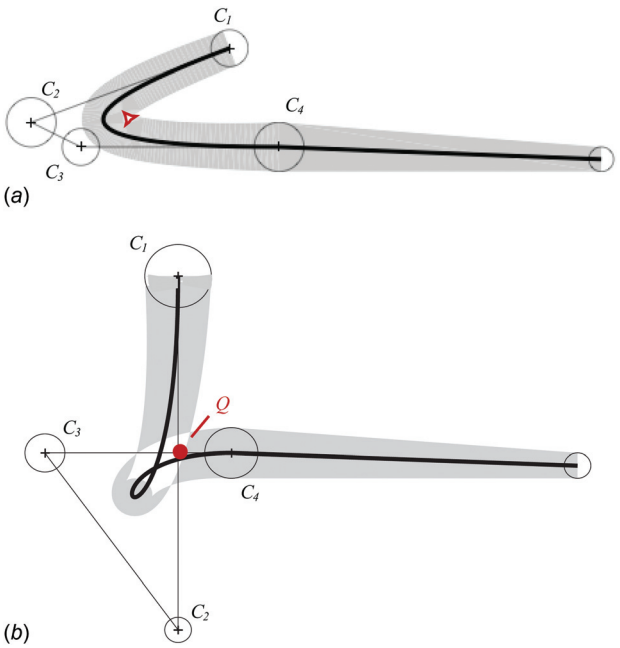

Fig. 6 Certain combinations of design variables result in the keel shape intersecting itself, creating a design that is not physically meaningful. Constraints were imposed to prevent cases like those shown here from being included in the optimization: (*a*) self-intersection constraint violation and (*b*) loop constraint violation.

where $\sigma_{allow} \equiv \sigma_y/F.S.$ with $F.S.$, the factor of safety, equal to 2 in this case. The maximum stress in the structure, σ_{max}, was found through finite element analysis.

2.4 Evaluating Lower Leg Trajectory Error. For the simple foot architectures shown in Fig. 2 that were previously optimized for LLTE, the deformation of the foot under a given load could be calculated analytically. Thus, each $x_{knee,n}^{model}$, $y_{knee,n}^{model}$, and $\theta_{knee,n}^{model}$ calculation in Eq. (1) was computationally inexpensive, so it was possible to find these values for every time interval during a step for which data were available. Using Winter's published data set and only considering the portion of stance for which the ankle angle is less than 90 deg, there are data for a total of $N = 26$ time intervals, all of which were used in calculating the LLTE during optimization of the simple architectures in Fig. 2.

For the shapes of prosthetic feet considered in this work, there is no analytical solution to find the deformation of the foot structure in response to a given load. Rather, finite element analysis is required. To evaluate the LLTE for a single design, finite element analysis (FEA) must be performed N times to calculate the deformation at each of the N time intervals. Since FEA is computationally expensive, it is advantageous to minimize the number of time intervals required. To determine how many time intervals were necessary and which instances during the step best represented the step as a whole, the LLTE optimization was performed for the simple analytical prosthetic foot models in Fig. 2 using each possible subset of the 26 total data points. It was found that with $N = 5$, the optimal design variable values were each within 5% of those values found using all 26 data points if the five data points used were at 33%, 48%, 60%, 74%, and 81% of stance, where 0% is heel strike, 24% is the instant at which the ankle begins to dorsiflex past a neutral position, and 100% is toe-off (Fig. 7). As an example of the data used as model inputs and target outputs, the ground reaction forces and the positions of the lower leg segment for three of these five time intervals from Winter's data are shown in Fig. 8. For a given foot design, FEA was performed on the foot five times, once for each of the five time intervals.

The x, y, and θ coordinates of the knee and lower leg segment can be found from just the position of the node at which the GRFs were applied, given by (x_{load}, y_{load}) and the position of a node at the tip of the foot, (x_{end}, y_{end}), where each of those positions refer to the deformed foot under loading. For the purposes of this calculation, the end node to which (x_{end}, y_{end}) refers was a virtual point added to the FEA model at a position of 20 cm anterior to the ankle. This was 5 cm beyond the end of the physical foot, but provided a useful point that could be used to calculate the angle of the ground relative to the foot in the ankle-knee reference frame, particularly when the center of pressure was very close to the tip of the physical foot. Because the toe of the foot was unconstrained and the only external loads were the ground reaction forces, there were no internal bending moments within the foot structure between the point at which the GRFs are applied and the tip of the finite element model of the foot. Consequently, this portion of the foot is undeformed, and the bottom of the foot distal to the loading point remains straight. For the center of pressure between the foot and the ground to indeed be at the node at which the loads have been applied, this entire segment of the foot, between the load point and the end of the foot, must be flat on the ground. The virtual end point on the finite element model does not affect these results; it only makes the length of the segment in contact with the ground longer, making the calculation of the angle of that segment more accurate. This is true as long as the center of pressure is proximal to the very end of the physical foot. When the center of pressure is at the end of the foot, the foot is only in point contact with the ground and can rotate rigidly about that point, so the position of the prosthesis is underconstrained by just the ground reaction forces and center of pressure and cannot be calculated from the ground reaction forces and center of pressure position without additional assumptions. Thus, only the portion of stance right up until the center of pressure reaches this point is included in the optimization.

The angle between the ground and the horizontal in the ankle-knee reference frame in which the FEA was performed, and, equivalently, the angle of the lower leg segment with respect to vertical in the global reference frame, was calculated from the FEA results as

$$\theta_{LL} = \tan^{-1}\left(\frac{y_{end} - y_{load}}{x_{end} - x_{load}}\right) \tag{9}$$

as shown in Fig. 9.

In the global reference frame, the origin was defined as the point of intersection between the ankle-knee axis and the ground

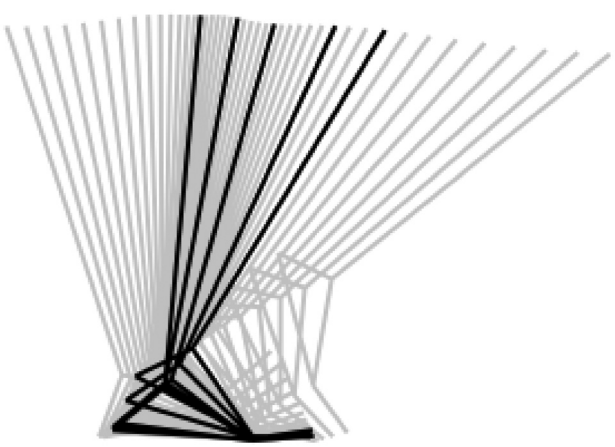

Fig. 7 Of the 43 time intervals during stance included in Winter's published gait data [21] shown in gray, the foot is flat on the ground and the ankle is in dorsiflexion for 26. Of those 26, the five shown in black were found to best represent the entire step. When these five data points were used, the optimal design variable values for each of the two degree-of-freedom analytical models in Fig. 2 were each within a maximum difference of 5% of the optimal design variable values as found when all 26 available data points were used.

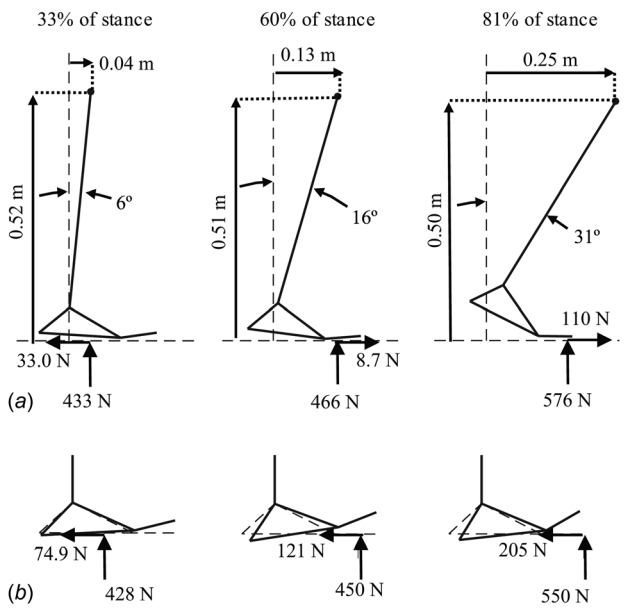

Fig. 8 Free body diagrams of the GRFs on the feet and the lower leg position during three of the five time intervals used in the finite element LLTE evaluation: (*a*) global reference frame and (*b*) ankle-knee reference frame

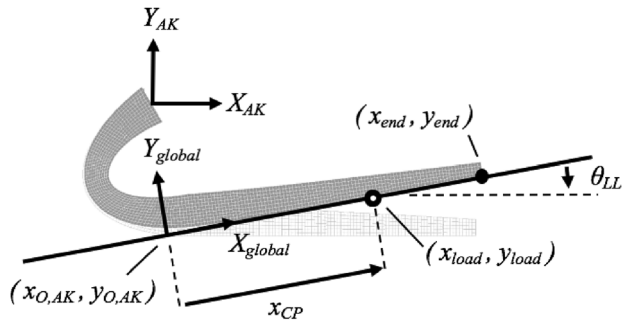

Fig. 9 Example of a deformed foot result from the FE model in the ankle-knee reference frame with the variables used in Eqs. (9)–(11) labeled. The variables X_{AK}, Y_{AK}, X_{global}, and Y_{global} denote the *x*- and *y*-axes of the ankle-knee reference frame and the global reference frame, respectively.

when the ankle-knee axis is perpendicular to the ground during stance. Because the center of pressure data used as an input to the model is measured in the global reference frame, the x-coordinate of the center of pressure in the global reference frame is the distance between the center of pressure and the origin of the global reference frame along the ground. Then the coordinates of the global origin in the ankle-knee reference frame, $x_{O,\mathrm{AK}}$ and $y_{O,\mathrm{AK}}$ are given by

$$\begin{bmatrix} x_{O,AK} \\ y_{O,AK} \end{bmatrix} = \begin{bmatrix} x_{\mathrm{load}} - x_{cp}\cos\theta_{LL} \\ y_{\mathrm{load}} - x_{cp}\sin\theta_{LL} \end{bmatrix} \tag{10}$$

Finally, the position of the knee in the global reference frame was found by taking the vector from the global reference frame origin to the knee in the global reference frame, then rotating the vector by θ_{LL} (Fig. 10). That is

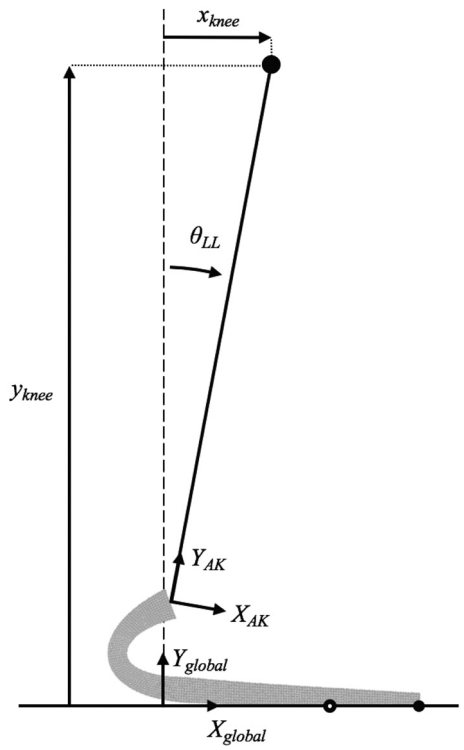

Fig. 10 Deformed foot finite element results from Fig. 9 rotated into the global reference frame. The variables x_{knee}, y_{knee}, and θ_{LL} shown here for the modeled foot are input into Eq. (1) to compare these resulting kinematics to the target physiological data.

$$\begin{bmatrix} x_{\mathrm{knee}} \\ y_{\mathrm{knee}} \end{bmatrix} = \begin{bmatrix} \cos\theta_{LL} & \sin\theta_{LL} \\ -\sin\theta_{LL} & \cos\theta_{LL} \end{bmatrix} \cdot \begin{bmatrix} x_{AK} - x_{O,AK} \\ y_{AK} - y_{O,AK} \end{bmatrix} \tag{11}$$

where x_{AK} and y_{AK} are the coordinates of the knee in the ankle-knee reference frame, so $x_{\mathrm{AK}} = 0$ and $y_{\mathrm{AK}} = L_{\mathrm{AK}}$, with L_{AK} the length of the shank between the ankle and the knee, which is the distance from the knee to the ground in the input physiological data set minus the height of the prosthetic foot, h, for the particular design in consideration.

To automate the LLTE calculation for a particular design to allow for optimization, a custom MATLAB script was used to write and save text files containing input batch commands for adina, the commercially available FEA software used in this optimization. The commands within the text files defined the foot geometry as a two-dimensional plane stress solid, meshed the surfaces using nine-node elements with edge length 2 mm, defined the material properties, and applied the appropriate loads. The displacement and strain options for the solver were left to their default value, which allows the solver to determine whether large or small displacement and strain formulations are more appropriate. A boundary condition was applied at the ankle to fix all degrees-of-freedom, as the analysis was performed in the ankle-knee reference frame, so any external loads would be opposed by reaction forces and moments at the ankle point, where the prosthetic foot would connect to the rest of the prosthesis. The finite element analysis was run via command line prompts executed through MATLAB. The results, namely the deformed position of the load node and the end node, were saved in another text file, which was read and processed via another custom MATLAB script, which calculated the $x_{\mathrm{knee},n}^{\mathrm{model}}$, $y_{\mathrm{knee},n}^{\mathrm{model}}$, and $\theta_{LL,n}^{\mathrm{model}}$ corresponding to that load case using Eqs. (9)–(11). This was repeated for the other four load cases. Finally, the $x_{\mathrm{knee},n}^{\mathrm{model}}$, $y_{\mathrm{knee},n}^{\mathrm{model}}$, and $\theta_{LL,n}^{\mathrm{model}}$ and the target physiological $x_{\mathrm{knee},n}^{\mathrm{phys}}$, $y_{\mathrm{knee},n}^{\mathrm{phys}}$, and $\theta_{LL,n}^{\mathrm{phys}}$ values for all five cases were used with Eq. (1) to calculate the LLTE value for that set of design variables.

2.5 Optimization Problem Formulation. The following optimization problem was solved to design the foot:

$$\left.\begin{aligned} \min_X: \quad & \mathrm{LLTE}(X) \\ \text{subject to}: \quad & \max(0.5w_c - \rho) \le 0 \\ : \quad & \left(\frac{\overline{lC_1C_2}}{\overline{lQC_1}} - \frac{4}{3}\right)\left(\frac{\overline{lC_2C_3}}{\overline{lQC_2}} - \frac{4}{3}\right) - \frac{4}{9} \le 0 \\ : \quad & C_{3d} - C_{4d} \le 0 \\ : \quad & \sigma_{\max} - \sigma_{\mathrm{allow}} \le 0 \end{aligned}\right\} \tag{12}$$

The optimization was performed using a hybrid of MATLAB's built-in genetic algorithm function and pattern search optimization function. The objective function was a custom script, which returned the LLTE value of a particular design following the previously described method. A custom mutation function was used in the genetic algorithm to increase the likelihood of valid mutations within the design variable bounds. The default mutation function in MATLAB for a bounded problem attempts a single random mutation without regards to bounds, then only uses this mutation in the next generation if all bounds happen to be met. If any one of the design variables is outside of its bounds, the mutation is not used. The original design is passed on to the next generation unchanged. This results in premature convergence on local minima. The custom mutation function changed each variable individually by a random amount selected from a normal distribution, similar to the default MATLAB mutation function for unbounded optimization problems. To account for the bounds, the standard deviation for one side of the normal distribution was

decreased when a design variable was very close to one of its bounds such that it was unlikely that a mutated design variable would exceed the bound. If it did exceed the bound, that design variable was set equal to the bound it exceeded in the following generation.

This mutation function increased the diversity of designs explored through the genetic algorithm, increasing the likelihood that the optimal design found by the algorithm was indeed the global minimum. To further ensure this was the case, the optimization was repeated five times to check that each of the optimal designs returned were nearly identical.

2.6 Prototype Fabrication and Finite Element Model Validation. Once the optimal keel design was found, a heel and a surface to attach the ankle of the foot to the rest of the prosthesis were incorporated. The heel was designed to be as thin as possible while maintaining a minimum factor of safety of two on the structure so that the bending of the heel beam would mimic early stance plantarflexion. The thickness of the heel beam was approximated by analytically calculating the thickness that would result in a factor of safety of two at the base of the heel beam. A heel beam of the calculated thickness was then added to the finite element model of the foot. The maximum heel strike ground reaction force from Winter's gait data was applied to the finite element model, and the resulting stress calculated. The thickness of the heel beam was adjusted until the minimum factor of safety in the structure was approximately equal to two.

The ankle of the finite element model foot used in the optimization was rigidly fixed to the rest of the prosthetic leg. To best replicate this condition without increasing the height of the foot more than necessary, material was added to the ankle portion of the foot, creating a horizontal surface to which a male pyramid adapter, the standard attachment method for prosthetic components, could be affixed.

Finally, the toe and heel of the foot were rounded in response to feedback obtained during previous testing of the simple prototypes shown in Fig. 3. According to subjects, the rounded heel and toe allow for smoother transitioning to and from the prosthetic foot, as well as improved maneuverability. The vertical thickness of the foot was adjusted to maintain the same bending stiffness in the toe despite the change in width into the plane of the page (from the reference of looking at the profile of the foot).

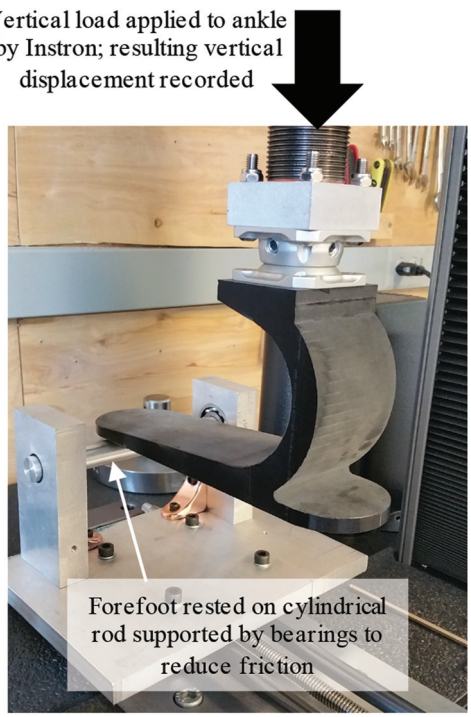

Fig. 11 Experimental setup used to measure vertical displacement of the forefoot in response to applied vertical loading up to 658 N to validate finite element model of foot

The prototype was machined from nylon 6/6 and a male pyramid adapter was attached to the ankle. An Instron material testing machine was used to measure the displacement of the prosthetic foot in response to loading and verify that the finite element analysis accurately modeled the prosthetic foot. To constrain the position of the load acting on the foot, the forefoot was placed on a cylindrical rod mounted on rotational bearings in a jig rigidly affixed to the lab bench (Fig. 11). This setup ensured the contact load on the forefoot would be normal to the face of the rod. The vertical load applied by the Instron was increased from 0 N to 658 N. At regular intervals during loading, the vertical displacement and the angle of the forefoot relative to the fixed circular rod were measured and recorded. The forefoot angle was used to calculate the horizontal load acting on the foot, as the Instron controls and records only vertical loads.

The measured vertical loads and calculated horizontal loads at seven different instances throughout loading were applied to the finite element model of the foot, including the heel and ankle attachment surface. A fully fixed boundary condition was applied to the surface of the ankle to which the male pyramid adapter was attached. The vertical displacement of the load point in response to these loads was computed and compared to the equivalent value measured during Instron testing.

2.7 Preliminary Testing in India. Prototype feet were brought to India for qualitative testing at BMVSS to determine whether there were any obvious shortcomings of the methodology or this particular foot that needed to be addressed before an extensive study could be performed to quantitatively evaluate the foot. A total of six subjects with unilateral transtibial amputation, all of whom had at least one year of experience using the Jaipur Foot, were fit with the prototype. The subjects walked around a room with a smooth, tiled floor until they were comfortable with the foot. They were then asked to go up and down stairs and ramps, then finally outside to walk on uneven surfaces. This testing lasted no more than one hour. After completing these activities, the subjects provided qualitative assessments of the prototype. Quantitative metrics, such as Likert scales, were not used, as experience has shown that subjects at BMVSS, most of whom are illiterate and have little to no formal education, are unfamiliar with the concept of numerical ratings, even if the numbers are replaced by textual descriptions (e.g., very bad, bad, ok, good, very good, etc.). Consequently, results from such studies are unreliable and can be misleading. However, if asked to qualitatively compare a prototype foot to his or her own prosthetic foot, the subjects are able to provide insightful responses that are informative for future design iterations.

3 Results

With the initial bounds given in Eqs. (3) and (4), the optimal design resulting from the optimization was

$$X = [0.0791, 0.0307, -0.1499, 0.0725 \quad 0.0357, \\ -0.1488, 0.0135, 0.0169, 0.1010]$$

with an LLTE value of 0.145. However, this design extended 12.2 cm posterior to the ankle, far too much to fit in a standard shoe (Fig. 12). The lower bounds on C_{2x} and C_{3x} were then increased from –0.15 m to –0.07 m to limit the length of the foot in the posterior direction. Additionally, the upper bound on C_{2y} was decreased from 0.10 m to 0.00 m to force the foot to not extend above the ankle, which would make attaching the foot to the rest of the prosthesis difficult. With these new bounds, the optimization was run again, yielding an optimal design of

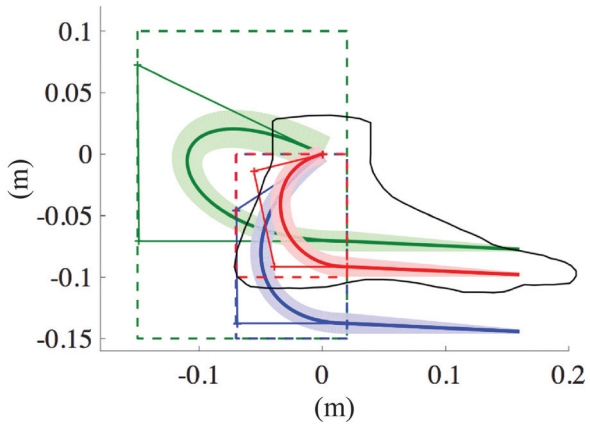

Fig. 12 Optimal keel designs found through the wide Bézier curve optimization method. The initial bounds resulted in a foot with an LLTE value of 0.145 (shown in green), but too large to fit within the envelope of a biological foot (shown in black). The subsequent designs, shown in blue, and finally in red, have higher LLTE values, at 0.153 and 0.186, respectively, but only the final optimal design (red) meets the size and shape requirements of a prosthetic foot that can be used in daily life. Note that in this figure, the three designs and the outline of the foot are aligned by the ankle position as defined in Sec. 2.1. The length of the pylon connecting the user's socket to the ankle of the foot would be adjusted to ensure the length of the prosthetic-side leg was equal to that of the biological leg.

$$X = [0.1461, 0.0142, -0.0698, -0.0455 \quad 0.0202, \\ -0.0690, 0.0156, 0.0170, 0.1031]$$

with an LLTE value of 0.153. The optimal design no longer extended too far posterior to the ankle, but was very tall, with the vertical distance from the bottom of the foot to the ankle, h, nearly 15 cm. This would preclude users with long residual limbs from using the foot. To obtain the final optimal result, the upper bound for h was decreased from 0.15 m to 0.10 m, producing an optimal design of

$$X = [0.996, 0.0142, -0.0556, -0.0139 \quad 0.0178, \\ -0.0389, 0.0160, 0.0162, 0.1034]$$

which had an LLTE value of 0.186 and fits completely within the envelope of a biological foot. The maximum stress in this final optimal design was 41.3 MPa, for a minimum factor of safety of 2.00. The position of the modeled lower leg segment for this final optimal design, as calculated using finite element analysis, is compared to the target physiological lower leg trajectory in Fig. 13.

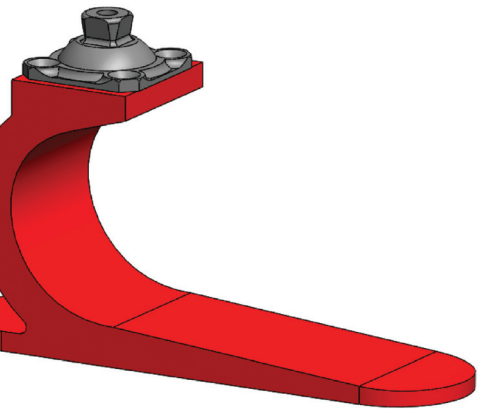

Fig. 14 Solid model of foot based on optimal design, with added heel and male pyramid adapter to attach the foot to the rest of the prosthesis

A heel and ankle attachment surface were designed following the method described above (Fig. 14). The foot was machined from nylon 6/6 and weighed 368 g. Using the supplier-provided elastic modulus defined in Sec. 2.2 of $E = 2.41$ GPa, the FEA solution gave a vertical displacement of 4.0 cm under a vertical load of 658 N applied at a horizontal distance of 13 cm from the ankle, 0.5 cm more than the Instron-measured displacement of 3.5 cm (Fig. 15). The elastic modulus of the material was later measured to be $E = 2.54$ GPa. With this measured modulus, the FEA solution gave a vertical displacement of 3.8 cm under the same vertical load, reducing the difference between the FEA and measured results to 0.3 cm.

Subjects who tested the foot provided mixed feedback. Younger subjects who prioritized mobility over stability liked the foot's energy storage and return compared to the Jaipur foot, which returns very little energy to the user. One subject commented that he could not run with the Jaipur Foot, but could with the prototype. Older subjects and some particularly cautious younger subjects felt unstable on the prototype. Most subjects liked the reduced weight of the prototype relative to the Jaipur Foot, which weighs between 800 g and 1 kg; however, one subject commented that because of the lighter weight, he was afraid the foot would break. All subjects commented that they would need a cosmetic cover for the prototype to make it look like a biological foot before they could use it daily. The doctors who run BMVSS and the authors agreed that the negative comments were all either related to the particular subject not being a candidate for an energy storage and return-type foot, which are typically only prescribed to more active subjects, or to the prototype being very different from the Jaipur Foot, which the subjects had been using for

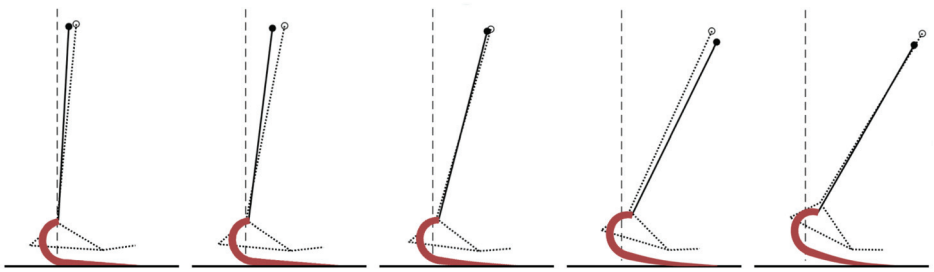

Fig. 13 Lower leg trajectory for the final optimal compliant foot (red foot design in Fig. 12, solid line showing lower leg trajectory here) compared to the target physiological lower leg trajectory (dotted line) for each of the five loading scenarios considered. The physiological data show the position of the markers at the knee, ankle, heel, metatarsal, and toe as collected during typical, unimpaired walking. Because these markers were placed at physical locations on the subject's foot, there is space between the markers and the ground in the physiological data.

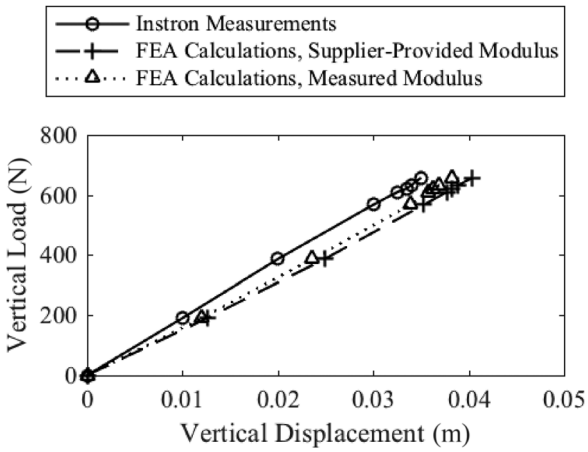

Fig. 15 Comparison of Instron-measured and FEA-calculated vertical displacements under loads applied at a horizontal distance of 13 cm from the ankle for both the supplier-provided elastic modulus, $E = 2.41$ GPa, and the measured elastic modulus, $E = 2.54$ GPa

a minimum of 10 years and a maximum of 47 years. None of the feedback necessitated significant changes to the design. The BMVSS doctors and the authors agreed that the foot will be ready for an extended field trial over the course of several weeks as soon as a cosmetic cover is incorporated. This cosmetic cover must both look like a biological foot and be able to withstand harsh environments, such as barefoot use on rough terrain and submersion in water.

4 Discussion

To contextualize the optimal design from this wide Bézier curve optimization, the LLTE-optimal designs for the simple foot architectures shown in Fig. 2 had LLTE values of 0.269 for the rigid circular foot, 0.172 for the foot with the rotational ankle and metatarsal joints, and 0.187 for the foot with a rotational ankle joint and a cantilever beam forefoot when evaluated using the same fives loading scenarios as were used for the single part prototype. The first two optimal designs of the single part keel (green and blue curves in Fig. 12) had smaller LLTE values than any of the simple foot architectures, so they would better replicate the target physiological lower leg trajectory under the five loading scenarios used. When the size of the single part keel was constrained to fit within the envelope of a biological foot, the LLTE value increased to 0.186, approximately equivalent to the simple foot with the rotational ankle and cantilever beam forefoot, and slightly larger than that for the foot with rotational ankle and metatarsal joints. However, the single part keel was the only foot that met the critical requirement of being smaller than a biological foot, which would allow it to fit within a cosmetic and protective cover and be used in shoes. Therefore, this slight decrease in performance is necessary to produce a prosthetic foot for daily use. Additionally, because the wide Bézier curve design does not require multiple parts, such as a spring, axis of rotation, or rigid structural elements, it can be made significantly lighter than either of the articulated simple architectures presented. Multiple experimental prototypes have been made to replicate the optimal designs of the simple architectures while minimizing the mass of the foot, such as those shown in Fig. 3, but the minimum mass achieved was 980 g, approximately 2.7 times the mass of the wide Bézier curve foot. Furthermore, the method presented here yields a design that is much easier to manufacture than the prototypes with articulated ankle joints, as the wide Bézier curve foot consists of a single nylon part that could easily be injection molded or extruded.

The genetic algorithm optimization took an average of 15 h, 1 min, and 44 s to run. The subsequent pattern search optimization took an additional 1 h, 38 min and 51 s on average. Evaluating the LLTE value for a single design took an average of 6.06 s. The primary purpose of this work was to develop a framework to use wide Bézier curve parameterization and a combination of MATLAB scripts and ADINA FEA software to produce a single-part prosthetic foot with a minimal LLTE value.

The following limitations to this work affected the general applicability of the resulting optimal foot, but were not addressed here because they would increase the optimization run time. Further analyses will be performed in the future to determine which of these limitations impact the results significantly enough to merit the additional optimization time that would be required to resolve them. The complexity of the final design was limited by the definition of the design space, as was shown in Fig. 4. In future work, a more comprehensive design space will be explored by adding complexity with additional design variables, such as using higher order Bézier curves to define the shape of the foot. The heel could also be incorporated into the optimization rather than optimizing the keel and forefoot and then designing a heel around that structure. Loading scenarios from early stance plantarflexion, when the center of pressure is posterior to the ankle, could then be included in the LLTE evaluation. Similarly, the surface to which the male pyramid adapter was attached could be included to improve the accuracy of the boundary conditions on the finite element model.

The shape of the foot has been optimized based on only five loading scenarios that are assumed to be adequately representative of the entire step. The lower leg trajectory of the prosthetic foot designed through the optimization may better replicate physiological gait kinematics throughout the whole step if more loading scenarios are included. The optimization runtime should scale linearly with the number of loading scenarios included, as each LLTE evaluation would perform an additional FEA simulation for each additional loading scenario, and the LLTE evaluation time is dominated by the FEA simulations. The number of function evaluations would not change significantly so long as the rate of convergence was not affected by the number of loading scenarios. Future work may include using more than five loading scenarios to determine if and how much the optimal design is affected.

Another potential source of error that could limit how accurately the FEA represents the kinematics of the foot during actual use is the direction of the GRF applied on the FE model. The input GRFs were measured in the global reference frame, then translated into the ankle-knee reference frame based on the orientation of the lower leg in the physiological data set to be applied to the ankle-knee reference frame-based FE model. The orientation of the ankle-knee reference frame of the wide Bézier curve foot during a particular load scenario depends on the deformed shape of the foot, which is dependent on the direction of the applied load. Thus, if and only if the foot deforms in such a way as to exactly replicate the orientation of the ankle-knee reference frame in the physiological data set, that is, $\theta_{LL,n}^{\text{model}} - \theta_{LL,n}^{\text{phys}} = 0$ in Eq. (1), the loading in the FEA is exactly equivalent to that in the input physiological gait data when both are rotated back into the global reference frame. Otherwise, the GRF magnitude is equivalent, but it is rotated by an amount equal to $\theta_{LL,n}^{\text{model}} - \theta_{LL,n}^{\text{phys}}$ relative to the GRF as measured in the global reference frame. For the optimal wide Bézier curve foot design presented here, the loading was rotated by a maximum of 4.18 deg relative to the direction of the GRF measured in the global reference frame. This source of error could be eliminated through iteratively solving for the orientation of the ankle-knee reference frame for the wide Bézier curve foot. This iterative process would have to be repeated for each loading scenario, with each iteration requiring an additional FEA simulation until the orientation of the ankle-knee reference frame used to calculate the loads applied to the FE model converged with the ankle-knee reference frame found from the deformed shape of the foot. This would consequently significantly increase the runtime of the LLTE evaluation for a single design, but would most

likely not affect the number of evaluations required for the optimization.

Because a set of published gait data for a single person was used both for the input kinetic data and for the target kinematic data, the optimal design is valid only for people of similar body mass and leg lengths as the subject with whom the data were recorded. After preliminary testing on subjects of similar size to clinically validate the method presented here, the method can be applied using sets of gait data for various body masses and leg lengths to produce a range of prosthetic feet to accommodate all potential users. Further, the input data can easily be adjusted proportionally to different users' body weight and size. The flexibility of the design and optimization presented here may enable the creation of customized, three-dimensional printed prosthetic feet for specific individuals.

5 Conclusions

The shape and size of a prosthetic foot was optimized as a compliant mechanism with the objective of minimizing the LLTE compared to able-bodied values. The forefoot was parameterized as a wide Bézier curve with constraints imposed such that only physically meaningful shapes were considered. The deformed shape of each foot design was calculated for five different loading scenarios representative of different phases of stance using ADINA finite element analysis software, run through a custom MATLAB script. From the deformed shape of the foot, the position of the knee and the orientation of the lower leg segment were found and used to evaluate the LLTE for that particular design. A hybrid of the genetic algorithm and pattern search optimization functions built into the MATLAB optimization toolbox was used to perform the optimization. The final optimal design had an LLTE value similar to previously analyzed articulated prototypes, but unlike these prototypes, the compliant foot fit within the envelope of a biological foot, a critical requirement for a daily-use prosthetic foot. Furthermore, at 368 g, the optimal foot was less than half the weight of the articulated prototypes. The single-part design compliant foot is also far easier to manufacture.

The resulting design was built and tested on an Instron material testing machine to demonstrate that the finite element analysis used to optimize the foot indeed matched the physical foot. Under a load of 682 N applied at a horizontal distance of 13 cm from the ankle, the maximum difference between the Instron-measured vertical displacement and finite element results was 0.3 cm, or 9% of the FEA predicted displacement, which is within the expected error of the measurement apparatus. The foot was tested qualitatively with our partner organization in India, which revealed no major design flaws. In the near future, a cosmetic and protective cover will be built for the foot so that an extended field trial can be conducted for more feedback in how the foot performs in daily activities.

Acknowledgment

This work was made possible by funding from the MIT Tata Center for Technology and Design. The authors would like to thank Dr. Caroline Hargrove and her team at McLaren Applied Technologies, Victor Prost at MIT, and Dr. Pooja Mukul, Dr. M. K. Mathur, and D. R. Mehta from BMVSS for their support.

References

[1] Arya, A. P., Lees, A., Nirula, H. C., and Klenerman, L., 1995, "A Biomechanical Comparison of the SACH, Seattle and Jaipur Feet Using Ground Reaction Forces," Prosthet. Orthot. Int., **19**(1), pp. 37–45.
[2] Nederhand, M. J., Van Asseldonk, E. H. F., van der Kooij, H., and Rietman, H. S., 2012, "Dynamic Balance Control (DBC) in Lower Leg Amputee Subjects; Contribution of the Regulatory Activity of the Prosthesis Side," Clin. Biomech., **27**(1), pp. 40–45.
[3] Klodd, E., Hansen, A., Fatone, S., and Edwards, M., 2010, "Effects of Prosthetic Foot Forefoot Flexibility on Gait of Unilateral Transtibial Prosthesis Users," J. Rehabil. Res. Develop., **47**(9), pp. 899–910.
[4] Klodd, E., Hansen, A., Fatone, S., and Edwards, M., 2010, "Effects of Prosthetic Foot Forefoot Flexibility on Oxygen Cost and Subjective Preference Rankings of Unilateral Transtibial Prosthesis Users," J. Rehabil. Res. Develop., **47**(6), pp. 543–552.
[5] Bonnet, X., Villa, C., Fode, P., Lavaste, F., and Pillet, H., 2014, "Mechanical Work Performed by Individual Limbs of Transfemoral Amputees During Step-to-Step Transitions: Effect of Walking Velocity," Proc. Inst. Mech. Eng. Part H, J. Eng. Med., **228**(1), pp. 60–66.
[6] Adamczyk, P. G., and Kuo, A. D., 2015, "Mechanisms of Gait Asymmetry Due to Push-Off Deficiency in Unilateral Amputees," IEEE Trans. Neural Syst. Rehabil. Eng., **23**(5), pp. 776–785.
[7] Major, M. J., Kenney, L. P., Twiste, M., and Howard, D., 2012, "Stance Phase Mechanical Characterization of Transtibial Prostheses Distal to the Socket: A Review," J. Rehabil. Res. Develop., **49**(6), pp. 815–829.
[8] Zelik, K. E., Collins, S. H., Adamczyk, P. G., Segal, A. D., Klute, G. K., Morgenroth, D. C., Hahn, M. E., Orendurff, M. S., Czerniecki, J. M., and Kuo, A. D., 2011, "Systematic Variation of Prosthetic Foot Spring Affects Center-of-Mass Mechanics and Metabolic Cost During Walking," IEEE Trans. Neural Syst. Rehabil. Eng., **19**(4), pp. 411–419.
[9] Houdijk, H., Pollmann, E., Groenewold, M., Wiggerts, H., and Polomski, W., 2009, "The Energy Cost for the Step-to-Step Transition in Amputee Walking," Gait Posture, **30**(1), pp. 35–40.
[10] Linde, V. D., Cheriel, J., and Alexander, C. H., 2004, "A Systematic Literature Review of the Effect of Different Prosthetic Components on Human Functioning With a Lower-Limb Prosthesis," J. Rehabil. Res. Develop., **41**(4), pp. 555–570.
[11] Hafner, B. J., 2005, "Clinical Prescription and Use of Prosthetic Foot and Ankle Mechanisms: A Review of the Literature," J. Prosthet. Orthotics, **17**(4), pp. S5–S11.
[12] Hofstad, C., van der Linde, H., van Limbeek, J., and Postema, K., 2004, "Prescription of Prosthetic Ankle-Foot Mechanisms After Lower Limb Amputation (Review)," Cochrane Database Syst. Rev., **1**, p. CD003978.
[13] Fey, N. P., Klute, G. K., and Neptune, R. R., 2011, "The Influence of Energy Storage and Return Foot Stiffness on Walking Mechanics and Muscle Activity in below-Knee Amputees," Clin. Biomech., **26**(10), pp. 1025–1032.
[14] Hansen, A. H., Childress, D. S., and Knox, E. H., 2000, "Prosthetic Foot Roll-Over Shapes With Implications for Alignment of Transtibial Prostheses," Prosthet. Orthotics Int., **24**(3), pp. 205–215.
[15] Hansen, A. H., and Childress, D. S., 2005, "Effects of Adding Weight to the Torso on Roll-Over Characteristics of Walking," J. Rehabil. Res. Develop., **42**(3), p. 381.
[16] Hansen, A. H., and Childress, D. S., 2004, "Effects of Shoe Heel Height on Biologic Rollover Characteristics During Walking," J. Rehabil. Res. Develop., **41**(4), pp. 547–554.
[17] Hansen, A. H., Childress, D. S., and Knox, E. H., 2004, "Roll-Over Shapes of Human Locomotor Systems: Effects of Walking Speed," Clin. Biomech., **19**(4), pp. 407–414.
[18] Olesnavage, K. M., and Winter V, A. G., 2018, "A Novel Framework for Quantitatively Connecting the Mechanical Design of Passive Prosthetic Feet to Lower Leg Trajectory," IEEE Trans. Neural Syst. Rehabil. Eng., (in press).
[19] Olesnavage, K. M., and Winter V, A. G., 2015, "Lower Leg Trajectory Error: A Novel Optimization Parameter for Designing Passive Prosthetic Feet," IEEE International Conference on Rehabilitation Robotics (ICORR), Singapore, Aug. 11–14, pp. 271–276.
[20] Olesnavage, K. M., 2018, "Development and Validation of a Novel Framework for Designing and Optimizing Passive Prosthetic Feet Using Lower Leg Trajectory," Ph.D. thesis, Massachusetts Institute of Technology, Cambridge, MA.
[21] Winter, D. A., 2009, *Biomechanics and Motor Control of Human Movement*, Wiley, Hoboken, NJ.
[22] Olesnavage, K. M., and Winter, V, A., G., 2016, "Design and Preliminary Testing of a Prototype for Evaluating Lower Leg Trajectory Error as an Optimization Metric for Prosthetic Feet," ASME Paper No. DETC2016-60565.
[23] Olesnavage, K. M., and Winter, V, A., G., 2015, "Design and Qualitative Testing of a Prosthetic Foot With Rotational Ankle and Metatarsal Joints to Mimic Physiological Roll-Over Shape," ASME Paper No. DETC2015-46518.
[24] Howell, L. L., 2001, *Compliant Mechanisms*, Wiley, New York.
[25] Lyu, N., and Saitou, K., 2005, "Topology Optimization of Multicomponent Beam Structure Via Decomposition-Based Assembly Synthesis," ASME J. Mech. Des., **127**(2), pp. 170–183.
[26] Saxena, A., and Ananthasuresh, G. K., 1999, "Topology Synthesis of Compliant Mechanisms for Nonlinear Force-Deflection and Curved Path Specifications," ASME J. Mech. Des., **123**(1), pp. 33–42.
[27] Lu, K. J., and Kota, S., 2006, "Topology and Dimensional Synthesis of Compliant Mechanisms Using Discrete Optimization," ASME J. Mech. Des., **128**(5), pp. 1080–1091.
[28] Bruns, T. E., and Tortorelli, D. A., 2001, "Topology Optimization of Non-Linear Elastic Structures and Compliant Mechanisms," Comput. Methods Appl. Mech. Eng., **190**(26–27), pp. 3443–3459.
[29] Santer, M., and Pellegrino, S., 2009, "Topological Optimization of Compliant Adaptive Wing Structure," Am. Inst. Aeronaut. Astronaut. J., **47**(3), pp. 523–534.
[30] Frecker, M. I., Ananthasuresh, G. K., Nishiwaki, S., Kikuchi, N., and Kota, S., 1997, "Topological Synthesis of Compliant Mechanisms Using Multi-Criteria Optimization," ASME J. Mech. Des., **119**(2), pp. 238–245.

[31] Cao, L., Dolovich, A. T., and Zhang, W. C., 2015, "Hybrid Compliant Mechanism Design Using a Mixed Mesh of Flexure Hinge Elements and Beam Elements Through Topology Optimization," ASME J. Mech. Des., **137**(9), p. 092303.
[32] Deepak, S. R., Dinesh, M., Sahu, D. K., and Ananthasuresh, G., 2009, "A Comparative Study of the Formulations and Benchmark Problems for the Topology Optimization of Compliant Mechanisms," ASME J. Mech. Rob., **1**(1), p. 011003.
[33] Xu, D., and Ananthasuresh, G. K., 2003, "Freeform Skeletal Shape Optimization of Compliant Mechanisms," ASME J. Mech. Des., **125**(2), pp. 253–261.
[34] Lan, C. C., and Cheng, Y. J., 2008, "Distributed Shape Optimization of Compliant Mechanisms Using Intrinsic Functions," ASME J. Mech. Des., **130**(7), p. 072304.
[35] Hetrick, J. A., and Kota, S., 1999, "An Energy Formulation for Parametric Size and Shape Optimization of Compliant Mechanisms," ASME J. Mech. Des., **121**(2), pp. 229–234.
[36] Zhou, H., and Ting, K.-L., 2006, "Shape and Size Synthesis of Compliant Mechanisms Using Wide Curve Theory," ASME J. Mech. Des., **128**(3), pp. 551–558.